Wind and Structures, *Vol. 31, No. 3 (2020) 217-227*
DOI: https://doi.org/10.12989/was.2020.31.3.217

Influence of non-Gaussian characteristics of wind load on fatigue damage of wind turbine

Ying Zhu*[1,2] and Miao Shuang[3a]

[1]*Railway Engineering Research Institute, China Academy of Railway Sciences Corporation Limited, Beijing 100081, China*
[2]*State Key Laboratory for Track Technology of High-speed Railway, Beijing 100081, China*
[3]*State Nuclear Electric Power Planning Design & Research Institute Corporation Limited, Beijing 100095, China*

(*Received September 5, 2019, Revised January 13, 2020, Accepted March 9, 2020*)

Abstract. Based on translation models, both Gaussian and non-Gaussian wind fields are generated using spectral representation method for investigating the influence of non-Gaussian characteristics and directivity effect of wind load on fatigue damage of wind turbine. Using the blade aerodynamic model and multi-body dynamics, dynamic responses are calculated. Using linear damage accumulation theory and linear crack propagation theory, crack initiation life and crack propagation life are discussed with consideration of the joint probability density distribution of the wind direction and mean wind speed in detail. The result shows that non-Gaussian characteristics of wind load have less influence on fatigue life of wind turbine in the area with smaller annual mean wind speeds. Whereas, the influence becomes significant with the increase of the annual mean wind speed. When the annual mean wind speeds are 7 m/s and 9 m/s at hub height of 90 m, the crack initiation lives under softening non-Gaussian wind decrease by 10% compared with Gaussian wind fields or at higher hub height. The study indicates that the consideration of the influence of softening non-Gaussian characteristics of wind inflows can significantly decrease the fatigue life, and, if neglected, it can result in non-conservative fatigue life estimates for the areas with higher annual mean wind speeds.

Keywords: non-Gaussian wind; wind field simulation; translation model; direction wind; wind-induced fatigue

1. Introduction

From the natural vibration frequency perspective, dynamical characteristics of wind turbines can be compared to high-rise buildings with a low frequency and heights ranging from 60 to160 meters. Because the comfort level is not considered in the current design codes, the wind-induced vibrations of wind turbines may produce large vibrations at moderate and frequent wind velocities. Thus, structures may undergo a great number of stress cycles leading to damage accumulation and can determine structural failure without exceeding design wind actions. For obtaining more stable wind speeds and powerful unit, the current trend of wind turbines is to reach higher into the atmosphere. Moreover, due to the coupled model of rotating blades and tower under wind loading (Ilhan *et al*. 2018, Ke *et al*. 2019), and the control systems which ensures wind turbines operate within the design range (such as yaw the turbine, start or stop the turbine, and keep the rotational speed and the power output within a certain range), dynamical behavior of wind turbines exhibits obvious non-linearity. Therefore, it is necessary to evaluate the wind-induced fatigue damage and life of wind turbines based on the coupled blade-tower dynamic response and control systems of the structure.

In current design standards (IEC61400-1 2005) and analysis tools (Jonkman B. and Jonkman J. 2005, Larsen and Hansen 2005) of wind turbines, the wind turbulence inflows specified are usually modeled as stationary random Gaussian processes, normally ignoring the influence of high-order statistical moments of wind inflows (Do *et al*. 2015). Generally, the Gaussian hypothesis is appropriate for wind inflows associated with flat and even terrain. However, the measurement data (Fragoulis 1997, Nielsen *et al*. 2004, Hui *et al*. 2017) show that the wind turbulence in complex terrain exhibits strongly non-Gaussian characteristics. Moreover, previous studies show that building structures and coastal engineering under non-Gaussian wind inflows will have a greater wind-induced response and will accelerate fatigue damage compared with the Gaussian case (Kareem and Zhao 1994, Lutes and Sarkani 2004).

Fatigue evaluation subjected to wind loads can be treated by using two approaches: cycle counting method (Nieslony 2009) in which calculations proceed in the time domain and the spectral method (Braccesi *et al*. 2015) in which calculations proceed in the frequency domain. For the spectral method, some frequency domain formulations have been established in recent study to determine the wind-excited fatigue of slender vertical structures subjected to along-wind (Robertson *et al*. 2004, Repetto and Solari 2012, Ding and Chen 2015a, Zhu and Tian 2018), cross-wind (Solari 2002, Chen 2014), and simultaneous along-wind and cross-wind vibrations (Solari 2004). Such

*Corresponding author, Ph.D.
E-mail: zhuying0727@hotmail.com
[a]Ph.D.
E-mail: shuangmiao204@163.com

http://www.techno-press.com/journals/was&subpage=7
ISSN: 1226-6116 (Print), 1598-6225 (Online)

approaches take into account the joint probability distribution of the mean wind speed, the mean fatigue damage and life under the assumption of the narrow band Gaussian hypothesis (Lynn and Stathopoulos 1985). Comparison with time-domain approach, numerical results (Benasciutti and Tovo 2006a, 2006b) indicate that the narrow band Gaussian hypothesis can lead to large overestimates of the wind-induced fatigue, when the quasi-static part of the response is not negligible and the non-Gaussian characteristic of wind inflows is not considered. Based on these, the time-domain approach, which is appropriate for evaluating the fatigue damage subjected to non-Gaussian wind loads (Xu 1995) or when the nonlinear behavior of the structure must be taken into account (Ding *et al*. 2016), is used to assess fatigue damage and life of wind turbines under wind inflows in this study.

In formulas of wind loads, mean and standard deviation of fluctuating wind load are proposed in codes, and the non-linear part of wind loads is neglected. Therefore, if a structure is under high turbulence intensity, the peak factor and fatigue damage may be underestimated, since contribution of the non-linear part of wind loads is large and the response is non-Gaussian. For the softening non-Gaussian characteristics, Kareem (Kwon and Kareem 2011) and Chen (Chen and Huang 2009), based on the Hermite moment model, estimated the extreme value using the peak factor method. On the basis of above researches, Ding (Ding and Chen 2015b) presented the revised and simplified formulas of the peak factor method. Chen (Ding and Chen 2015c) improved the frequency-domain fatigue analysis method under non-Gaussian wind load based on the orthogonal polynomials and Hermite moment model. In terms of researches on the influence of wind turbines under non-Gaussian wind inflows, most of the existing achievements (Binh *et al*. 2008, Gong and Chen 2014, Shuang and Song 2018) focus on the extreme value response, lacking of the research on fatigue damage, particularly in the crack initiation stage and the crack propagation stage, which are taken into account under the condition of aeroelastic and control systems of wind turbines.

The wind turbine failures mostly focus on the blade root and welded connection at tower base (Chou and Tu 2011), while the composite material extensively used improves blade strength and fatigue life. Therefore, only the fatigue damage of the welded connection at tower base is considered. It should be noted that the aim of this paper is the assessment of the influence of non-Gaussian wind inflows and wind direction on fatigue damage and life of wind turbines, so the details of structure can be simplified. Considering the characteristics of structure and wind inflows, the section behavior of tower base subjected to uniaxial stress depends on the in-plane, out-of-plane bending stress and compressive stress caused by self-weight. Meanwhile, the bending stress at different positions in the critical section is related to the wind direction. Therefore, the effect of the wind direction cannot be neglected in the fatigue damage evaluation.

The paper is organized as follows. Section 2 introduces the relevant theory on stochastic processes and translation model for non-Gaussian processes, and then moment-based translation model is outlined in some detail, which forms a partial basis for the proposed method. In Section 3, wind inflows with non-Gaussian characteristic are generated by using translation process theory and spectral representation method, and dynamic response of wind turbine are calculated. The fatigue damage rate, the crack formation life and the crack growth life of wind turbine subjected to non-Gaussian inflows are discussed in Section 4 and Section 5, respectively. Finally, Section 6 summarizes the key findings.

2. Summary of existing theory

This section outlines the relevant elements of the non-Gaussian vector. Since the formulation for the non-Gaussian vector requires the transform process, the Hermite model and Moment-based model for expressing the non-Gaussian process are summarized in Section 2.1 and 2.2. These also serve as the foundation for the present work.

2.1 Hermite model for softening non-Gaussian vectors

According to the kurtosis, γ_4, the non-Gaussian vector can be divided into two categories, namely the softening vector ($\gamma_4 > 3$) and hardening vector ($\gamma_4 < 3$). Let U be a standard Gaussian vector with components u_i of zero mean and unit variance and consider a vector X of the same size as U. The non-Gaussian vectors X with components x_i of specified distribution F_i and correlation matrix can be generated by monotonically increasing transformations of the type as (Grigoriu 1984)

$$x_i = g\left(u_i\right) = F_{x_i}^{-1}\left[\Phi\left(u_i\right)\right] \tag{1}$$

where u_i is a standard Gaussian variable; x_i is a standard non-Gaussian variable; F_{xi} and $\Phi(\cdot)$ are the cumulative distribution functions (CDFs) of x_i and u_i respectively; and F_X^{-1} is the inverse function of F_{xi}. Multi-variate distributions obtained in this way are called translation systems.

The Hermite polynomials provide an analytical description of a nonlinear function g(u) in the translation system. Then, the non-Gaussian vector can be expressed as (Winterstein *et al.* 1994)

$$X = g(U) \approx \kappa\left[U + h_3(U^2 - 1) + h_4(U^3 - 3U)\right] \tag{2}$$

where κ and h_i are model coefficients, which can be obtained by fitting the translation function derived from CDF mapping or be approximately represented by empirical equations as (Kwon and Kareem 2011)

$$\begin{gathered}\kappa = \frac{1}{\sqrt{1+2h_3^2+6h_4^2}}; \quad h_3 = \frac{\gamma_3}{6}\left[\frac{1-0.015\left|\gamma_3\right|+0.3\gamma_3^2}{1+0.2(\gamma_4-3)}\right]; \\ h_4 = h_{40}\left[1-\frac{1.43\gamma_3^2}{\gamma_4-3}\right]^{1-0.1(\gamma_4)^{0.8}}; \quad h_{40} = \frac{\left[1+1.25(\gamma_4-3)\right]^{1/3}-1}{10}.\end{gathered} \tag{3}$$

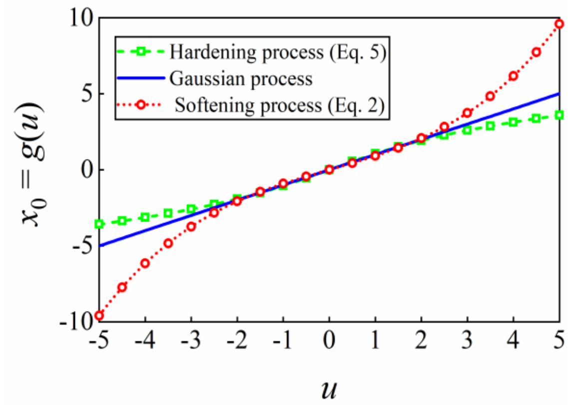

Fig. 1 Translation models of non-Gaussian processes

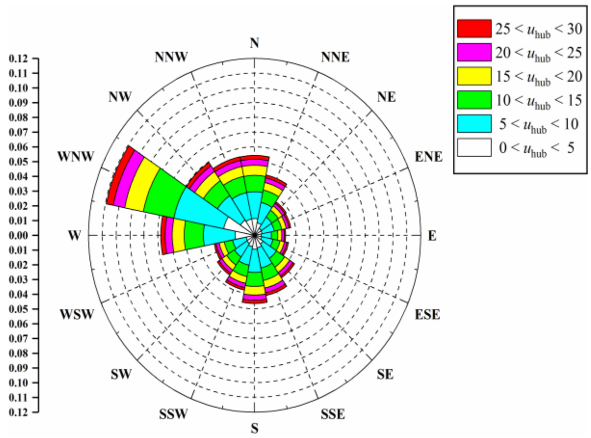

Fig. 2 Wind rose diagram

in which γ_3 and γ_4 are the skewness and kurtosis of the standardized non-Gaussian variable respectively. It should be noted that these expressions are intended for application in the ranges of $0<\gamma_4<12$ and $0 \le \gamma_3^2 \le (2\gamma_4)/3$.

2.2 Moment-based model for hardening non-Gaussian vectors

The hardening non-Gaussian processes with narrower distribution tails are often encountered in the dynamic response of operational wind turbines (Ding *et al*. 2013). The following Hermite model is widely used for modeling a standardized hardening non-Gaussian process through an underlying standard Gaussian process. However, the accuracy of these model coefficients is only ensured for representing very mildly hardening non-Gaussian processes (Winterstein 1988).

Generally, a random process can be expanded in terms of another random process through a set of orthogonal polynomials. The expansion of standard Gaussian process U in terms of a standard non-Gaussian process X should be expressed as follows by truncating higher terms (Ding and Chen 2015b):

$$U = g^{-1}(X) \approx b_2 X + b_3(X^2 - \gamma_3 X - 1) + b_4(X^3 - \gamma_4 X - \gamma_3) \tag{4}$$

where b_2, b_3 and b_4 are model coefficients.

The corresponding translation model from Gaussian to non-Gaussian variables is then determined as

$$X = g(u) \approx \left[\sqrt{\xi^2(U)+c} + \xi(U)\right]^{1/3} - \left[\sqrt{\xi^2(U)+c} - \xi(U)\right]^{1/3} - a \tag{5}$$

where $\xi(U)$, a, b and c are, respectively, expressed as

$$\xi(U) = \frac{U}{2b_4} + \frac{\gamma_3}{2} + a(1.5 + 1.5b - a^2); \quad a = \frac{b_3}{3b_4}; \quad b = \frac{(b_2 - b_3\gamma_3 - b_4\gamma_4)}{3b_4}; \quad c = (b-a^2)^3. \tag{6}$$

A least-square curve-fitting of the model coefficients as functions of skewness and kurtosis is performed, which leads to following closed-form expressions

$$b_2 = \varphi\left[1 - \frac{\gamma_3^4 + 1.2\gamma_3^2 - 0.18}{7.5\exp(0.5\gamma_4)}\right]; \quad b_3 = -\frac{0.8\gamma_3^5 + \gamma_3^3 + 0.77\gamma_3}{(\gamma_4-1)^2 + 0.5}; \quad b_4 = -\varphi\left[0.04 - \frac{11.5\gamma_3^4 + 6.8\gamma_3^2 + 3.5}{(\gamma_4^2+0.4)^2 + 0.15}\right]; \quad \varphi = \left[1 - 0.06(3-\gamma_4)\right]^{1/3}. \tag{7}$$

To ensure both the accuracy and monotone requirement of the translation function with the closed-form model coefficients, this region is approximated by

$$(1.35\gamma_3)^2 + 1.25 \le \gamma_4 \tag{8}$$

moment-based model calculated by Eqs. (2) and (5).

Fig.1 shows the translation models of non-Gaussian processes based on Hermite model and moment-based model calculated by Eq. (2) and Eq. (5).

3. The wind trubin and non-Gaussian wind inflows

3.1 The wind turbin and wind inflow characteristics

The wind turbine used in this study is an onshore 5-MW baseline wind turbine from National Renewable Energy Laboratory (NREL). The wind turbine with hub height of 90 meters and blade diameter of 126 meters is based on variable speed and pitch control system. The turbine is assumed to be land-based with a rigid foundation.

In the numerical example, the FAST code (Fatigue, Aerodynamics, Structures and Turbulence) was used to model the wind turbine with 24 DOFs, and structural-damping ratios are set to 0.477465 % critical in all modes of the isolated blade. The detail description of the model, material and aerodynamic parameters of blades and towers can be referred to the Reference (Jonkman *et al.* 2009).

The wind rose of meteorological data (mean wind speed and wind directions) used in this study is shown in Fig.2 The data series used were recorded between 2015 and 2018, which were provided by the NREL (Clifton 2016). As shown in the figure, the prevailing wind direction is WNW in the meteorological monitoring masts.

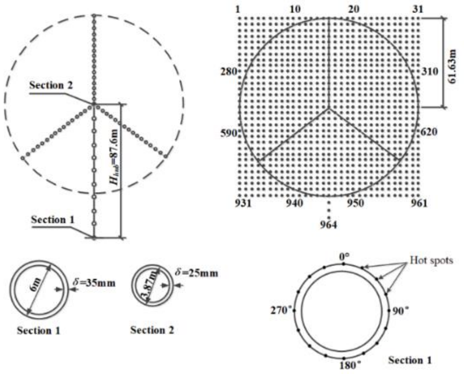

Fig. 3 The wind turbin and wind inflows

3.2 Fluctuating wind velocity

The wind turbulence field is simulated at 31 by 31 grid points with both height and width of 145 m and the single column grid points along the tower shown in Fig. 3. As shown in Fig. 3, the hub is located at the center of grid, and 964 times history of wind load will be simulated. Then, wind turbine design load condition 1.1 with normal turbulence model is chosen as the wind conditions for operational and parked turbines.

$$S_k(f) = \frac{4\sigma_k^2 L_k / \bar{u}_{\text{hub}}}{(1+6fL_k/\bar{u}_{hub})^{5/3}} \tag{9}$$

where f is angular frequency; u_{hub} is the mean wind speed at hub height; σ_k are standard deviations of turbulence wind speeds with σ_u=0.16(0.75u_{hub}+5.6), σ_v=0.8σ_u and σ_w=0.5σ_u; L_k are turbulence integral scales with L_u=8.1Λ_u, L_v=2.7Λ_u and L_w=0.66Λ_u; and turbulence scale coefficient (in unit of m) is Λ_u=0.7min(30, H_{hub}).

The coherence function defined by the complex magnitude of the cross-spectral density of the longitudinal wind speed components at two spatially separated points divided by the spectrum function can be expressed as (IEC 61400-1 2005)

$$coh_{ij,u}(f) = \exp\left[-a_u\sqrt{\left(\frac{f\cdot r}{\bar{u}_{hub}}\right)^2 + \left(b_u\cdot r\right)^2}\right] \tag{10}$$

where r is the magnitude of the projection of the separation vector between the two points on to a plane normal to the mean wind direction, and a_u and b_u are attenuation and offset coefficients with values a_u=12 and b_u=3.527×10^{-4} as defined in IEC 61400-1.

3.3 Wind field simulation

In this paper, the non-Gaussian and Gaussian wind fields are generated by transform model and the harmony superposition method (Rossi *et al.* 2004). In the operational condition, the mean wind speeds are divided into 12 bins from cut-in speed of 3 m/s to cut-out speed of 25 m/s with the bin width of 2 m/s. In the parked condition, the mean wind speeds are 1 m/s and 2 m/s lower than the cut-in

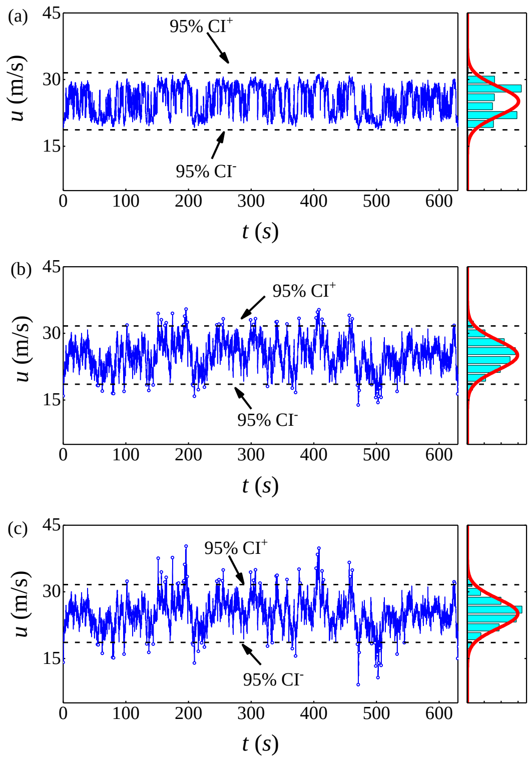

Fig. 4 Simulated wind speed time histories at the hub height: (a) hardening process, (b) Gaussian process, and (c) softening process

speed. In order to analyze the influence of the non-Gaussian characteristics of inflows, the skewness and kurtosis of wind fields take the values of 0 and 4.5 for the softening process and 0 and 1.5 for the hardening process, respectively. For considering the dispersion of samples, 50 wind turbulence time histories are simulated with duration of 630 s and time step of 0.05 s at each mean wind speed. Therefore, the analysis time step is 0.0125 s in dynamic analysis. For eliminating the influence of startup transient, the first 30 s of the dynamic response of wind turbine is removed.

Fig. 4 shows time histories of Gaussian and non-Gaussian wind fields at hub height with mean wind speed of 25 m/s. The dotted lines in the figure represent the mean value plus or minus 1.96 standard deviations which means 95% confidence interval for Gaussian distribution. The histogram reveals the probability density function of time histories of simulated wind speed, and the solid line is the PDF of Gaussian distribution with the same mean value and variance. It can be seen from the figure that both the softening and hardening wind fields show obvious non-Gaussian characteristics. Under the same target condition, the extreme value and quantity of those of the Gaussian wind field are between the hardening and softening processes.

The correlation coefficients of softening process and Gaussian process and of hardening process and Gaussian process are 0.99 and 0.96 in Fig. 4. So, the moment-based transform function maintains the correlation of three types of loads.

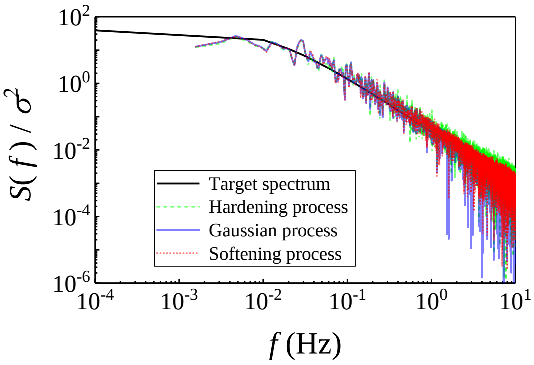

Fig. 5 Comparison between simulated spectrum and target spectrum

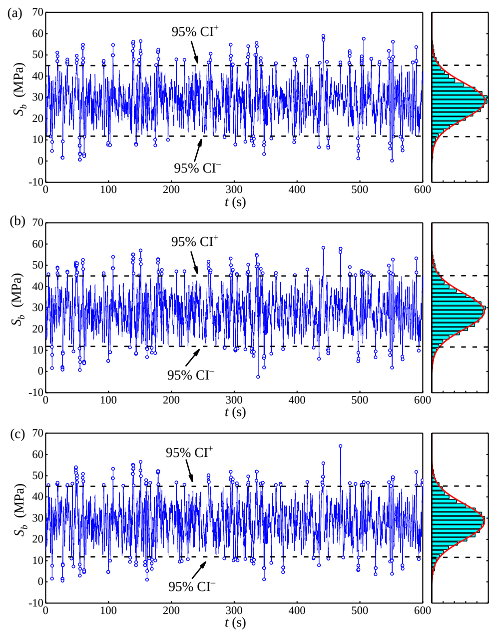

Fig. 6 Time histories of in-plane bending stress at tower base: (a) hardening process, (b) Gaussian process, (c) softening process

Fig. 5 compares the target spectrum with the simulated spectrum of the generated wind speed time histories, and the result shows that the PSDs of three different types of wind fields are in good agreement with the target spectrums.

4. Fatigue reliability analysis

4.1 Dynamic response of wind turbine

The FAST code is adopted to analyze the dynamic response of wind turbines, which is based on the coupled aerodynamic model of rotating blades and tower under wind loading and control systems. For considering the influence of the wind direction, the inflow is divided into 16 wind direction angles with increments of 22.5° as shown in Fig.2. It should be noted that the aerodynamic model and dynamic stall model are based on the blade element momentum theory (Leishman 2000) and the semi-empirical Beddoes-Leishman model (Leishman 1989, Leishman and Beddoes 1989). In this study, the critical section is defined as the welded connection at tower base, and hot spots are represented in Fig.3. Fig.6 shows time histories of in-plane bending stress of the hot spot (0 degree) subjected to Gaussian and non-Gaussian wind fields at mean wind speed of 25 m/s simulated by the same random seeds.

The total fatigue life of any detail generally consists of the crack initiation and crack propagation stages. The linear cumulative damage theory is used to evaluate the crack initiation life in this section, and the uncertainty of crack initiation life caused by structural parameters and load uncertainties are also taken into account. Meanwhile, the linear crack propagation theory is used to assess the crack propagation life in Section 5.

4.2 Fatigue damage with increasing mean wind speed

By using the rain-flow counting method, stress range S_{ri}, mean stress S_{mi} and the number of cycles N_i at stress range S_{ri} can be obtained. Then, the equivalent bending stress range neglecting any mean stress, based on the *S-N* curve, can be expressed as

$$S_{\mathrm{reff}}^{0}=\left(\sum_i f_i S_{ri}^{m}\right)^{1/m} \tag{11}$$

where m is the *S-N* curve slope, S_{ri} is i^{th} stress range and f_i is corresponding probability of occurrence.

According to Goodman's criterion, the equivalent stress range considering the effect of the mean stress, S_{reff}, can be expressed as

$$S_{\mathrm{reff}}=S_{\mathrm{reff}}^{0}\left(1-\frac{S_m}{S_u}\right)^{-1} \tag{12}$$

where S_m is the mean stress and S_u is the ultimate tensile strength.

According to the *S-N* curve, the number of stress cycles can be represented as

$$N_f=AS_{\mathrm{reff}}^{-m} \tag{13}$$

where A and m are parameters of the *S-N* curve with values m=3.0 and A=36.1×10^{10} MPa^3 for Detail Category E as defined in AASHTO. Since the threshold stress range is 31 MPa, fatigue life will not be affected by an effective stress range that is less than half of the threshold stress (S_{reff}<15.5 MPa) (Dowling 2007).

Based on the linear cumulative damage theory, fatigue damage within time t can be represented as

$$D(t)=\frac{v_0^{+}}{N_f}t \tag{14}$$

where v_0^{+} is the expected frequency of stress process.

Fig. 7 shows the comparison of equivalent stress of the hot spot and rotation speed with the increasing mean wind speeds subjected to Gaussian and non-Gaussian wind fields. It should be noted that the equivalent stress is obtained by

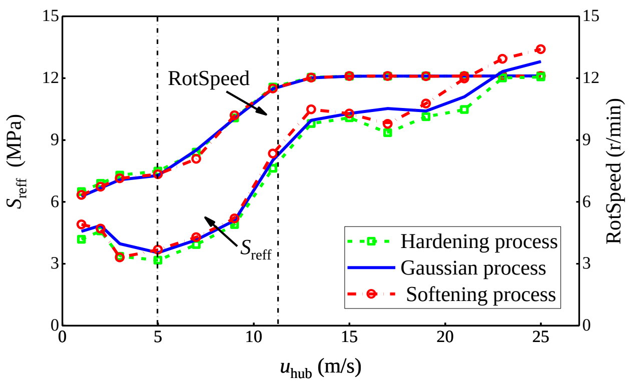

Fig. 7 Comparison of equivalent stress amplitudes and rotation speed (RotSpeed) with different mean wind speeds

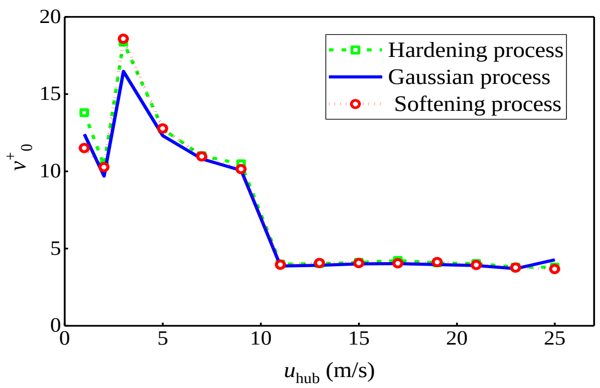

Fig. 8 Mean crossing rates with the increasing mean wind speeds

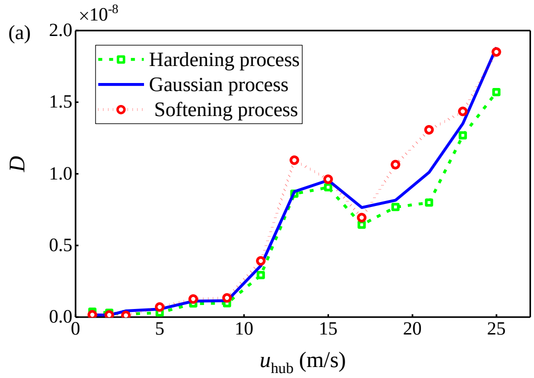

(a)

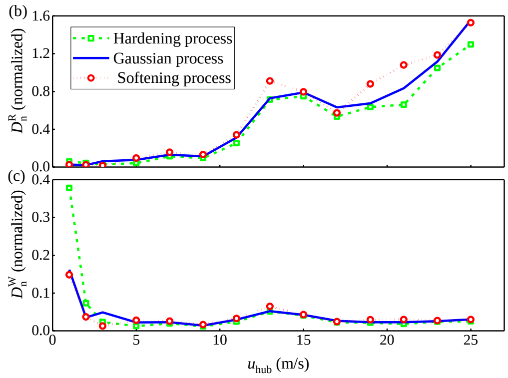

(b)

Fig. 9 Comparison of fatigue damage rate with the increasing mean wind speed: (a)fatigue damage rate (b) fatigue damage rate normalized by RotSpeed (c) fatigue damage rate normalized by wind speed

rain-flow counting method and Goodman's criterion. As expected, the equivalent stress amplitude and rotation speed increase with the mean wind speed increasing at hub height. It is evident that the equivalent stress decreases in sequence under softening, Gaussian and hardening wind fields. And rotation speed is not sensitive to the non-Gaussian characteristic of wind field. Meanwhile, the equivalent stress amplitude and rotation speed increase with the increasing mean wind speed before the rated wind speed of 11.4 m/s, and rotation speed maintains stable after exceeding the rated wind speed due to the variable-speed torque control. While, the equivalent stress amplitude maintains stable within a certain range, and it slowly rises when the mean speed is greater than 20 m/s. In addition, when the wind speed is lower than the cut-in speed, the blade does not generate power normally, and the wind load cannot be converted into the power. Therefore, the equivalent stress amplitude is larger than the cut-in wind speed.

The zero mean up-crossing rate of bending stress at the hot spot with the increasing mean wind speeds are shown in Fig. 8. It is observed that the v_0^+ are very close under wind fields with different probability characteristics. When wind speeds are in the range of the cut-in wind speed and rated speed, v_0^+ decreases rapidly with the increasing mean wind speed. When reaching the rated wind speed, v_0^+ is basically stable owing to the control system.

Fig. 9 shows the fatigue damage rate under Gaussian and non-Gaussian inflows with the mean wind speed increasing. It should be noted that the D_n^R and D_n^W represent fatigue damage rates normalized by RotSpeed and by ($C{\cdot}u_{\mathrm{hub}}^2$) in Fig. 9 (b) and (c). As shown in the figure, the fatigue damage rate is linear with respect to wind load which can be conceptually represented as $P = \rho u^2/2$, and it exhibits nonlinear relationship with rotation speed. Obviously, the effect of wind load exhibits relative importance after exceeding cut-in wind speed.

Since *S-N* curve is a significant nonlinear function of fatigue damage rate and equivalent stress amplitude, fatigue damage rates exhibit more obvious distinction than equivalent stress amplitudes, and the trend is consistent with equivalent stress amplitudes. Meanwhile, fatigue damage rates are minuteness when the mean wind speed is less than the cut-in speed due to considering the fatigue limit. Within a certain range, when the mean wind speed reaches the rated wind speed, the fatigue damage rates remain relatively stable. While mean wind speed exceeds 20 m/s, the fatigue damage rates rapidly increase.

4.3 Fatigue damage with consideration of wind direction

Fig. 10 shows the mean fatigue damage rate of the hot spot in the critical section with wind angle of 0°. The in-plane bending stress respectively is tensile stress and

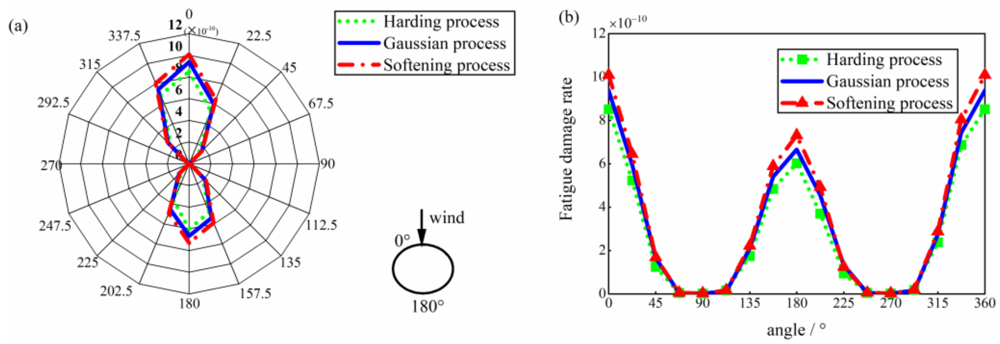

Fig. 10 Mean fatigue damage rate in the critical section with inflow direction of 0°

compressive stress at the point (0°) and the point (180°), and the mean stress caused by self-weight is compressive stress at the critical section. Since the Goodman criterion does not correct the compressive stress state, so the fatigue damage at the point (180°) is less than the point (0°).

4.4 Fatigue life of wind turbine

Based on the central limit theorem, it is assumed that the fatigue damage rate follows Gaussian distribution. Then, the mean value and variance of fatigue life at hot spot can be expressed as (Ding *et al.* 2016)

$$E[T_f]=\frac{1}{\mu_D}\left(1+\frac{\sigma_D^2}{2\mu_D}\right)T,$$
$$\mathrm{Var}[T_f]=\frac{\sigma_D^2}{\mu_D^3}\left(1+1.25\frac{\sigma_D^2}{\mu_D}\right)T^2. \tag{15}$$

where μ_D and σ_D are the mean and STD of fatigue damage of the critical section within time T, which can be represented as

$$\mu_D=\iint \mu_D(u_{ave},\theta)f(u_{ave},\theta)\mathrm{d}u_{ave}\mathrm{d}\theta,\quad \sigma_D =\iint \sigma_D(u_{ave},\theta)f(u_{ave},\theta)\mathrm{d}u_{ave}\mathrm{d}\theta. \tag{16}$$

where $\mu_D(u_{ave}, \theta)$ and $\sigma_D(u_{ave}, \theta)$ are the mean and standard deviation of fatigue damage obtained from 50 samples at each mean wind speed, and $f(u_{ave}, \theta)$ is the joint PDF of the mean wind speed and wind direction. According to IEC61400-1, the Rayleigh distribution can be used to model the probability distribution function of the mean wind speed, written as

$$f_U(u)=\frac{\pi u}{2u_{ave}^2}\exp\left[-\pi\left(\frac{u}{2}u_{ave}\right)^2\right] \tag{17}$$

where u_{ave} is annual mean wind speed.

The fatigue crack formation life at different annual mean wind speeds can be seen in Fig. 11. With the same stress mean value and variance, if the mean wind speed is smaller, due to the larger kurtosis of stress response under the softening wind field, the stress fluctuates near the mean value, and so there are more stress cycles less than the stress

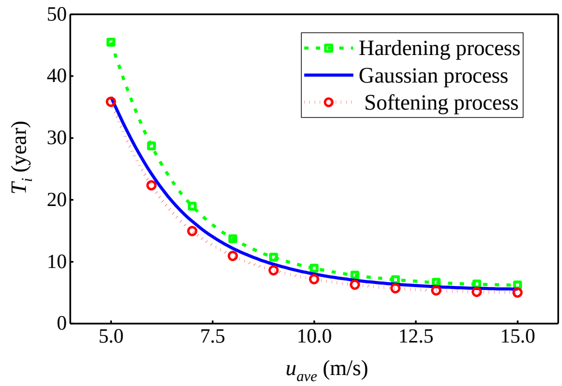

Fig. 11 Fatigue crack initiation life with different annual mean wind speeds

Table 1 Mean and STD of crack initiation life under three types of wind inflows with different annual mean wind speeds

u_{ave} (m/s)	wind inflows	$E[T_i]$ (year)	$\sigma[T_i]\times10^{-3}$ (year)
	Hardening	10.7	0.7
9	Gaussian	9.6	0.7
	Softening	8.6	0.4
	Hardening	18.9	1.2
7	Gaussian	16.5	1.1
	Softening	14.9	0.6
	Hardening	45.5	3.0
5	Gaussian	36.6	2.7
	Softening	35.8	1.4

amplitude threshold which cannot cause fatigue damage accumulation with consideration of the fatigue limit. Therefore, the crack formation life under softening wind field is not so far different with that of Gaussian wind field. With the increase of the mean wind speed, the stress amplitude under the softening wind field also increases gradually. The stress cycle amplitude lower than the stress amplitude threshold before gradually exceeds the stress amplitude threshold, and so the fatigue damage accumulation under the softening wind field is largest and the fatigue crack formation life is smallest. The results highlight the importance of the consideration of wind inflow with non-Gaussian characteristics when wind turbines are constructed in the area with higher annual mean wind speed.

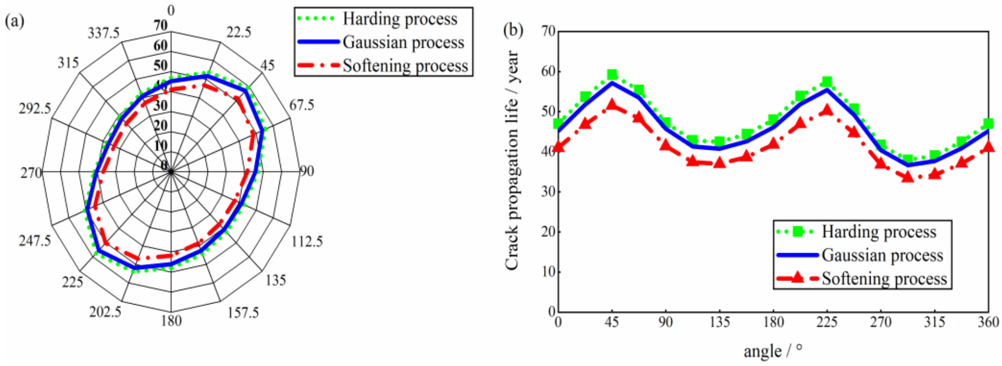

Fig. 12 The fatigue life considering wind direction of hot spots at the critical section

The mean value and STD of crack initiation life caused by the normal stress at the critical section under Gaussian and non-Gaussian wind fields are shown in Table 1. It can be seen that non-Gaussian wind fields have great influence on the crack formation life. The effect of non-Gaussian characteristics of wind inflows cannot be ignored in fatigue life estimation, especially, when wind turbines are located in the area with higher annual mean wind speeds or at higher hub height. Additionally, it is generally true that $\sigma_D(t)/\mu_D(t)$ decays like $[N(t)]^{-1/2}$ as $N(t)$ becomes large, in which $\sigma_D(t)$ represents only the uncertainty about damage due to the uncertainty about the stochastic time history. The fact that $\sigma_D(t)/\mu_D(t)$ becomes very small as t approaches T in most fatigue problems assures us that $\sigma_D(T)/\mu_D(T)$ is also very small, which allows us to ignore the discreteness of stress histories. It should be noted that the turbine acts as a low-pass filter which cuts off the high-frequency modes (Frandsen 2008). Then, the effect of non-Gaussian characteristic provides less sensitivity than that of parameter uncertainty as literature (Pagnini and Repetto 2011) shows in the fatigue life evaluation.

The fatigue crack formation life of hot spots caused by the normal stress in the critical section are shown in Fig. 12. It should be noted that the joint PDF of mean wind speed and wind direction is obtained by the NREL shown in Fig. 2. As shown in Fig. 2 and Fig. 12, the fatigue failure occurs at the position of the prevailing wind direction (WNW).

5. Crack propagation life

The presence of a crack can significantly reduce the strength of an engineering component due to brittle fracture. However, it is unusual for a crack of dangerous size to exist initially, although this can occur, as when there is a large defect in the material used to make a component. In a more common situation, a small flaw that was initially present develops into a crack and then grows until it reaches the critical size for brittle fracture. However, the fatigue crack propagation life is not accounted in present codes, so it is necessary to calculate the crack propagation life according to the fracture mechanics theory. Then, the remaining life can be calculated to determine whether the crack can be ignored, whether repair or replacement is needed immediately, or whether this can be postponed until a more convenient time.

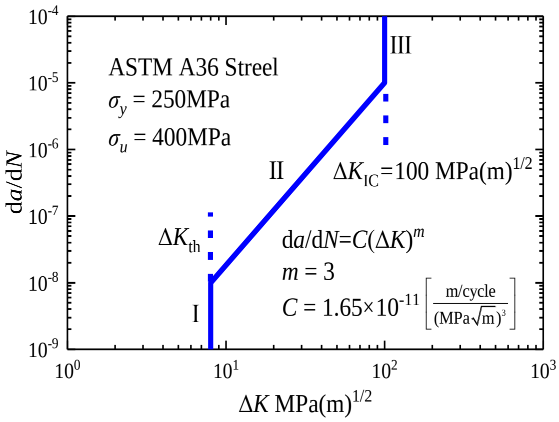

Fig. 13 Fatigue crack growth rates

Crack propagation is usually divided into instable propagation and subcritical propagation according to the rate of crack propagation. For a given material and a set of test conditions, the crack growth behavior can be described by the relationship between cyclic crack growth rate da/dN and stress intensity range ΔK. When the strength factor ΔK is less than its critical value ΔK_{IC}, crack growth rate da/dN can be determined by the Paris theorem

$$\frac{\mathrm{d}a}{\mathrm{d}N} = C(\Delta K_{\mathrm{reff}})^m \tag{18}$$

where C is crack growth rate coefficient; ΔK_{eff} is the intensity factor range of effective stress, which depends on the effective stress range and crack length as well as other geometric factors; and m is material constant.

By applying the Pairs formula, the number of cycles that the structure can withstand after the first initial crack for each annual mean wind speed is defined as

$$N_{if} = \frac{a_f^{1-m/2} - a_i^{1-m/2}}{C(F\Delta S\sqrt{\pi})^m(1-m/2)} \tag{19}$$

where a_f and a_i are final crack length and initial crack length, respectively; ΔS is effective stress range, and $\Delta S = S_{\mathrm{reff}}$; and F is dimensionless parameter about geometric shape and crack size, which is set equal to 1.12 when the ratio of crack length and component width is less than or equal to 0.4.

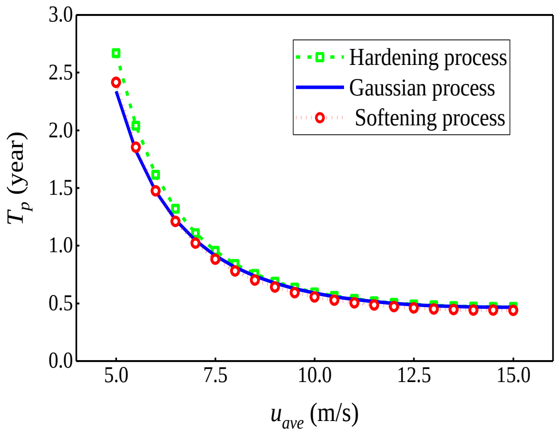

Fig. 14 Fatigue crack propagation life with different annual mean wind speeds

Based on a level 1 A in BS7910, the critical crack length can be represented as

$$a_f = a_c = \frac{1}{\pi}\left(\frac{0.707K_{\mathrm{IC}}}{S_{t,\max}}\right)^2 \tag{20}$$

where K_{IC} is the material toughness determined by the CVN Charpy impact test. $S_{t,\max}$ is the maximum tensile stress, and $S_{t,\max}$={SCF[S_{reff}/2-P/A]+σ_y}. SCF is the stress concentration factor, which is set equal to 1.5. P/A is compress stress owing to dead load. σ_y is yield strength of materials. In this study, the ASTM A36 steel is used, and material parameters are shown in Fig. 13.

Based on the PDF of the mean wind speed and stress cycles, crack growth life can be written as

$$T_f = \frac{1}{\sum \hat{D}_i P_i} \tag{21}$$

where $\hat{D}_i$ is the expected damage of the i^{th} mean wind speed over time T, i.e.

$$\hat{D}_i = \frac{v_0^+}{N_{if}} T \tag{22}$$

where N_{if} represents cycles of loading.

Fig. 14 shows the fatigue crack propagation life of hot spot with the increasing annual mean wind speed. Notably, crack propagation life of hot spot under non-Gaussian inflows are close to the life under Gaussian inflow, and crack propagation life decrease rapidly with increasing annual mean wind speed. That is because the maximum tensile stress takes into account yield strength of the material which is much larger than the equivalent stress amplitude. Therefore, it is reasonable to ignore the effect of non-Gaussian characteristics of wind inflows in the crack growth life assessment. In addition, compared with the crack formation life, the crack growth life can only be used as a safety reserve.

6. Conclusions

The presented study focuses on the effect of the non-Gaussian characteristics and wind direction of wind inflows on the fatigue life of wind turbines. The wind inflows are generated by the harmony superposition method and transformation process. Then, the dynamical responses of wind turbines under both Gaussian and non-Gaussian inflows are calculated by FAST code which considers the coupled model and control systems. The linear damage accumulation theory and the linear crack propagation theory are used to evaluate the fatigue crack initiation life and crack propagation life, respectively. An important assumption made in this study is that the tower base weld connection has no initial crack. After reaching its service life defined by the *S-N* curve, a though-thickness crack is allowed to develop with its initial length double the tower wall thickness. Based on the work presented in this paper, additional conclusions are as follows:

- The influence of non-Gaussian wind characteristics on fatigue damage rate of wind turbines becomes more significant with the increasing mean wind speed in the crack formation stage. Clearly, the non-Gaussian characteristics of wind field have negligible influence in the region with lower annual mean wind speed. However, with the annual mean wind speed increasing, the effect is gradually obvious. When the annual mean wind speed is 7m/s and 9m/s, the crack formation lifetime under softening non-Gaussian wind field decreases by about 10% compared with Gaussian process. The results highlight the importance of the consideration of wind inflow with non-Gaussian characteristics when wind turbines are constructed in the region with higher annual mean wind speed. In additional, the failure position of the crack initiation with consideration of wind directivity effect occurs at the prevailing wind direction.
- In the crack growth stage, the non-Gaussian wind field has little influence on the crack growth lifetime. Compared with the Gaussian process, the crack growth lifetime under the softening process decreases by about 4% on average. Therefore, the non-Gaussian characteristic of wind inflows is not considered in the crack propagation stage, and the crack propagation lifetime is regarded as the safety reserve of fatigue life.

Acknowledgements

The authors are grateful for the financial support received from science and technology research project of China railway corporation (No. 2017G006-A) and foundation project of China academy of railway sciences (No. 2018YJ048).

References

Benasciutti, D. and Tovo, R. (2006), “Comparison of spectral methods for fatigue analysis of broad-band Gaussian random processes”; *Probabilist. Eng. Mech.*, **21**(4), 287-299.

https://doi.org/10.1016/j.probengmech.2005.10.003.

Benasciutti, D. and Tovo, R. (2006), "Fatigue life assessment in non-Gaussian random loadings"; *Int. J. Fatigue*, **28**(7), 733-746. https://doi.org/10.1016/j.ijfatigue.2005.09.006.

Binh, L., Ishihara, T., Phuc, P. and Fujino, Y. (2008), "A peak factor for non-Gaussian response analysis of wind turbine tower"; *J. Wind Eng. Ind. Aerod.*, **96**(10-11), 2217-2227. https://doi.org/10.1016/j.jweia.2008.02.019.

Braccesi, C., Cianetti, F., Lori, G. and Pioli, D. (2015), "Random Multiaxial Fatigue: a comparative analysis among selected frequency and time domain fatigue evaluation methods"; *Int. J. Fatigue*, **74**, 107-118. https://doi.org/10.1016/j.ijfatigue.2015.01.003.

Chen, X. (2014), "Analysis of crosswind fatigue of wind-excited structures with nonlinear aerodynamic damping"; *Eng. Struct.*, **74**, 145-156. https://doi.org/10.1016/j.engstruct.2014.04.049.

Chen, X. and Huang, H. (2009), "Evaluation of peak resultant response for wind-excited tall buildings"; *Eng. Struct.*, **31**(4), 858-868. https://doi.org/10.1016/j.engstruct.2008.11.021.

Chou, J. and Tu, W. (2011), "Failure analysis and risk management of a collapsed large wind turbine tower"; *Eng. Fail Anal.*, **18**(1), 295-313. https://doi.org/10.1016/j.engfailanal.2010.09.008.

Clifton, A. (2016), "135-m Meteorological Towers at the National Wind Technology Center"

Ding, J. and Chen, X. (2015), "Fatigue damage evaluation of broad-band Gaussian and non-Gaussian wind load effects by a spectral method"; *Probabilist. Eng. Mech.*, **41**, 139-154. https://doi.org/10.1016/j.probengmech.2015.06.005.

Ding, J. and Chen, X. (2015), "Moment-based translation model for hardening non-Gaussian response processes"; *J. Eng. Mech.*, **142**(2), 6015006. https://doi.org/10.1061/(ASCE)EM.1943-7889.0000986.

Ding, J., Chen, X., Zuo, D. and Hua, J. (2016), "Fatigue life assessment of traffic-signal support structures from an analytical approach and long-term vibration monitoring data"; *J. Struct. Eng.*, **142**(6), 04016017. https://doi.org/10.1061/(ASCE)ST.1943-541X.0001475.

Ding, J., Gong, K. and Chen, X. (2013), "Comparison of statistical extrapolation methods for the evaluation of long-term extreme response of wind turbine"; *Eng. Struct.*, **57**, 100-115. https://doi.org/10.1016/j.engstruct.2013.09.017.

Do, T., Lindt, J. and Mahmoud, H. (2015), "Fatigue Life Fragilities and Performance-Based Design of Wind Turbine Tower Base Connections"; *J. Struct. Eng.*, **141**(7), 04014183. https://doi.org/10.1061/(ASCE)ST.1943-541X.0001150.

Dowling, N. (2004), *Mechanical Behavior of Materials*, Pearson Prentice Hall, Harlow, England.

Fragoulis, A. (1997), "The complex terrain wind environment and its effects on the power output and loading of wind turbines", 35th Aerospace Sciences Meeting and Exhibit.

Frandsen, S., Jørgensen, H.E. and Sørensen, J.D. (2008), "Relevant criteria for testing the quality of models for turbulent wind speed fluctuations"; *J. Sol. Engerg-T ASME*, **130**(3), 031016. https://doi.org/10.1115/1.2931511.

Gong, K. and Chen, X. (2014), "Influence of non-Gaussian wind characteristics on wind turbine extreme response"; *Eng. Struct.*, **59**, 727-744. https://doi.org/10.1016/j.engstruct.2013.11.029.

Grigoriu, M. (1984), "Crossings of non-Gaussian translation processes"; *J. Eng. Mech.*, **110**(4), 10-620. https://doi.org/10.1061/(ASCE)0733-9399(1984)110:4(610).

Hui, Y., Li, B., Kawai, H. and Yang, Q. (2017), "Non-stationary and non-Gaussian characteristics of wind speeds", *Wind Struct.*, **24**(1), 59-78. http://dx.doi.org/10.12989/was.2017.24.1.05.

IEC61400-1 (2005), *Wind turbines - part 1: Design requirements, International Electrotechnical Commission; Geneva*, Switzerland.

Ilhan, A., Bilgili, M. and Sahin, B. (2018), "Analysis of aerodynamic characteristics of 2 MW horizontal axis large wind turbine", *Wind Struct.*, **27**(3), 187-197. http://dx.doi.org/10.12989/was.2018.27.3.187.

Jonkman, B. and Jonkman, J. (2005), "FAST user's guide", National Renewable Energy Laboratory, Colorado.

Jonkman, J., Butterfield, S., Musial, W. and Scott, G. (2009), "Definition of a 5MW reference wind turbine for offshore system development", National Renewable Energy Laboratory, Colorado.

Kareem, A. and Zhao, J. (1994), "Analysis of non-Gaussian surge response of tension leg platforms under wind loads"; *J. Offshore Mech. Arct. Eng.*, **116**(3), 137-144. http://doi.org/10.1115/1.2920142.

Ke, S.T., Wang, X.H., and Ge, Y.J. (2019), "Wind load and wind-induced effect of the large wind turbine tower-blade system considering blade yaw and interference", *Wind Struct.*, **28**(2), 71-87. http://dx.doi.org/10.12989/was.2019.28.2.071.

Kwon, D. and Kareem, A. (2011), "Peak factors for non-Gaussian load effects revisited"; *J. Struct. Eng.*, **137**(12), 1611-1619. https://doi.org/10.1061/(ASCE)ST.1943-541X.0000412.

Larsen, T. and Hansen, A. (2005), "How 2 HAWC2 the user's manual", Wind Energy Division.

Leishman, J.G. (1989), "Modeling Sweep Effects on Dynamic Stall" *J. Am. Helicopter Soc.*, **34**(3), 18-29. https://doi.org/10.4050/JAHS.34.3.18.

Leishman, J.G. (2000), *Principles of Helicopter Aerodynamics*, Cambridge University Press, Cambridge, U.K.

Leishman, J.G. and Beddoes, T.S. (1989), "A Semi-Empirical Model for Dynamic Stall" *J. Am. Helicopter Soc.*, **34** (3), 3-17. https://doi.org/10.4050/JAHS.34.3.3.

Lutes, L. and Sarkani, S. (2004), *Random Vibrations: Analysis of Structural and Mechanical Systems*, Elsevier Inc, Burlington, Vermont, U.S.A.

Lynn, B. and Stathopoulos, T. (1985), "Wind-induced fatigue on low metal buildings", *J. Struct. Eng.*, **111**(4), 826-839. https://doi.org/10.1061/(ASCE)0733-9445(1985)111:4(826).

Nielsen, M., Larsen, G., Mann, J., Ott, S., Hansen, S. and Pedersen, B. (2004), "Wind simulation for extreme and fatigue loads", Risø-R-1437(EN), Risø National Lab, Denmark.

Nieslony, A. (2009), "Determination of fragments of multiaxial service loading strongly influencing the fatigue of machine components", *Mech. Syst. Signal Pr.*, **23**(8), 2712-2721. https://doi.org/10.1016/j.ymssp.2009.05.010.

Pagnini, L. and Repetto M.P. (2012), "The role of parameter uncertainties in the damage prediction of the alongwind-induced fatigue"; *J. Wind Eng. Ind. Aerod.*, **104-106**, 227-238. https://doi.org/10.1016/j.jweia.2012.03.027.

Repetto, M. and Solari, G. (2004), "Directional wind-induced fatigue of slender vertical structures", *J. Struct. Eng.*, **130**(7), 1032-1040. https://doi.org/10.1061/(ASCE)0733-9445(2004)130:7(1032).

Repetto, M. and Solari, G. (2012), "Closed-form prediction of the alongwind-induced fatigue of structures"; *J. Struct. Eng.*, **138**(9), 1149-1160. https://doi.org/10.1061/(ASCE)ST.1943-541X.0000543.

Robertson, A., Holmes, J. and Smith, B.W. (2004), "Verification of closed-form solutions of fatigue life under along-wind loading", *Eng. Struct.*, **26**(10), 1381-1387. https://doi.org/10.1016/j.engstruct.2004.05.004.

Rossi, R., Lazzari, M., and Vitaliani, R. (2004), "Wind field simulation for structural engineering purposes"; *Int. J. Numer. Meth. Eng.*, **61**(5), 738-763. https://doi.org/10.1002/nme.1083.

Shuang, M. and Song, B. (2018), "Reliability analysis of wind turbines under non-Gaussian wind load", *Struct. Des. Tall Spec.*, **27**(3), 1-17. https://doi.org/10.1002/tal.1443.

Solari, G. (2002), "The role of analytical methods for evaluating the wind-induced response of structures", *J. Struct. Eng.*, **90**, 12-15. https://doi.org/10.1016/S0167-6105(02)00264-7.

Winterstein S., Ede, T. and Kleiven, G. (1994), "Springing and slow-drift responses: predicted extremes and fatigue vs. simulation", *BOSS-94*, Cambridge.

Winterstein, S. (1988), "Nonlinear vibration models for extremes and fatigue", *J. Eng. Mech.*, **114**(10), 1772-1790. https://doi.org/10.1061/(ASCE)0733-9399(1988)114:10(1772).

Xu, Y. (1995), "Model-and full-scale comparison of fatigue-related characteristics of wind pressures on the Texas Tech building", *J. Wind Eng. Ind. Aerod.*, **58**(3), 147-173. https://doi.org/10.1016/0167-6105(95)00012-7.

Zhu, Y. and Tian, Y. (2018), "Fatigue Life Evaluation of Linear Structures with Uncertain-But-Bounded Parameters Under Stochastic Excitations"; *Int. J. Struct. Stab. Dy.*, **18**(3), 1850045. https://doi.org/10.1142/S0219455418500451.

AD